

Underscreening in concentrated electrolytes: Re-entrant swelling in polyelectrolyte brushes

Hayden Robertson,^{a#} Gareth R. Elliott,^a Andrew R. J. Nelson,^b Anton P. Le Brun,^b Grant B. Webber,^a Stuart W. Prescott,^c Vincent S.J. Craig,^d Erica J. Wanless,^a Joshua D. Willott^{a#}

^a College of Science, Engineering and Environment, University of Newcastle, Callaghan, NSW 2308, Australia

^b Australian Centre for Neutron Scattering, ANSTO, Locked Bag 2001, Kirrawee DC, NSW 2232, Australia

^c School of Chemical Engineering, UNSW Sydney, Sydney, NSW 2052, Australia

^d Department of Materials Physics, Research School of Physics, Australian National University, Canberra, ACT 0200, Australia

These authors contributed equally

Contents

Atomic force microscopy (AFM).....	3
Ellipsometry.....	4
Dry brush thickness maps.....	4
In situ solid-liquid measurements	6
Underscreening analysis.....	7
Defining the Debye-Hückel and re-entrant regions.....	7
Effective screening length calculation.....	7
Scaling analysis	8
Neutron Reflectometry	9
First moment.....	9
Full suite of NR data	9
MCMC spread of fits.....	11
KCl	11
MgCl ₂	14
LaCl ₃	17
YCl ₃	20
References.....	23

Atomic force microscopy (AFM)

Single molecule force spectroscopy (SMFS) measurements were performed using a Bruker Multimode VII Atomic Force Microscope (AFM) with a vertical engage J scanner in contact mode equipped with a closed fluid cell at 23 ± 2 °C. Measurements were performed using a V-shaped silicon nitride cantilever with a triangular tip of manufacturer quoted tip radius of 2-12 nm and a reflective gold backside coating (SNL-10, Bruker, USA). The cantilever spring constant was measured to be 0.067 N/m using the thermal tune method built into the instrument software. Before any measurements were performed, the fluid cell and O-ring were carefully cleaned with ethanol and MilliQ water and dried under a stream of nitrogen gas, and the cantilever cleaned via exposure to UV/O₃ for 15 min.

The experiments were conducted on a 158 Å PMETAC brush in 10 mM KCl at native pH of 6 using a ramp size of 1000 nm, at a tip velocity of 500 nm/s, and a constant maximum indentation load set sufficiently high to reach the constant compliance regime. Over 1000 force curves were measured across various locations of the brush, covering an area of 500 by 500 nm². Cantilever deflection vs displacement data of the resultant force curves were converted to normal force vs apparent separation curves using standard methods.¹ The wormlike chain (WLC) model was used to model the elastic behaviour of the single polymer chain during the final detachment (pull-off) event,²⁻⁴ and the results can be seen in Table S1 and Figure S1. Quoted errors are the standard deviation across all the curves used in the analysis. The software employed is readily available at <https://github.com/haydenrob/afmToolBox>.

Table S1: Results of the SMFS on a 158 Å PMETAC brush.

Persistence length (Å)	Contour length (Å)	Molecular weight (kg·mol ⁻¹)	Grafting density (×10 ⁻⁴ Å ⁻²)
4.07 ± 2.29	3980 ± 1090	275 ± 78	4.36 ± 1.24

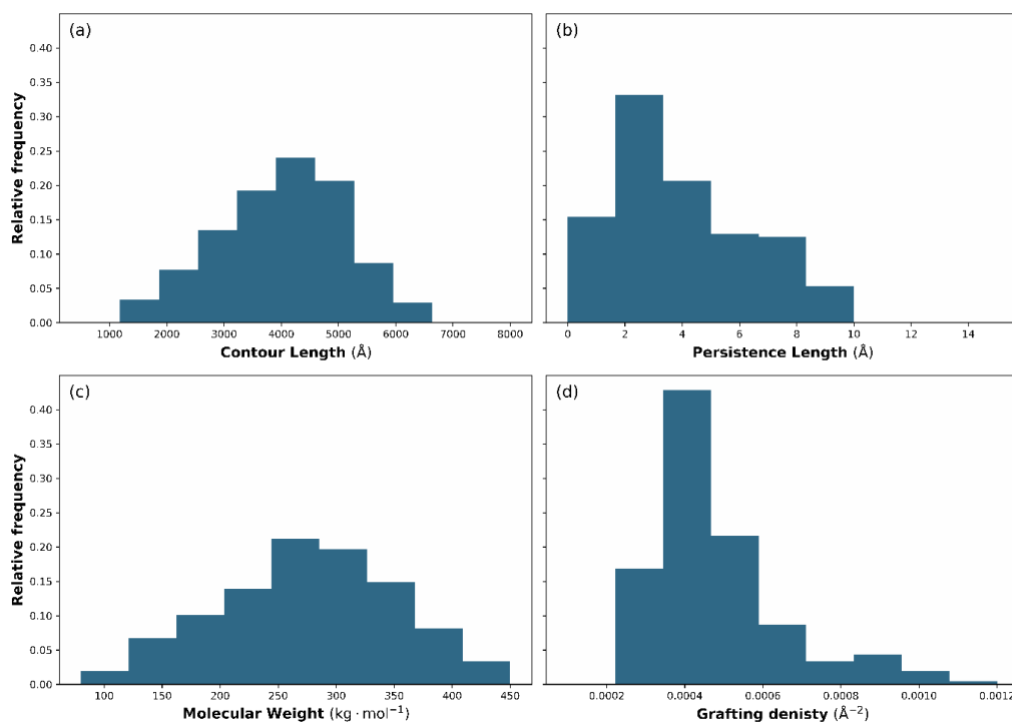


Figure S1: Histograms resulting from AFM SFMS studies: (a) contour length, (b) persistence length, (c) molecular weight and (d) grafting density.

Ellipsometry

Dry brush thickness maps

Here we present the areal thickness maps of the dry films used for all *in situ* spectroscopic ellipsometry measurements (Figure S2) and neutron reflectometry measurements (Figures S3). All data was processed with *refellips*,⁵ and all relevant data and code required to reproduce the figures can be found on the Zenodo repository^{6,7} and *refellips* GitHub repository www.github.com/refnx/refellips.

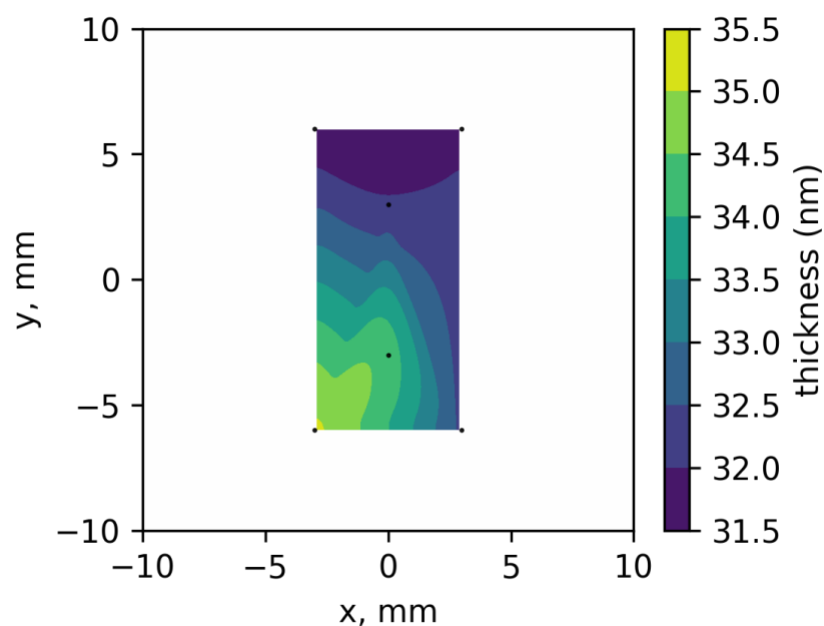


Figure S2: Areal thickness map of the 32.9 ± 1.3 nm PMETAC brush used for all *in situ* solid-liquid ellipsometry measurements. The map was determined by variable angle spectroscopic ellipsometry.

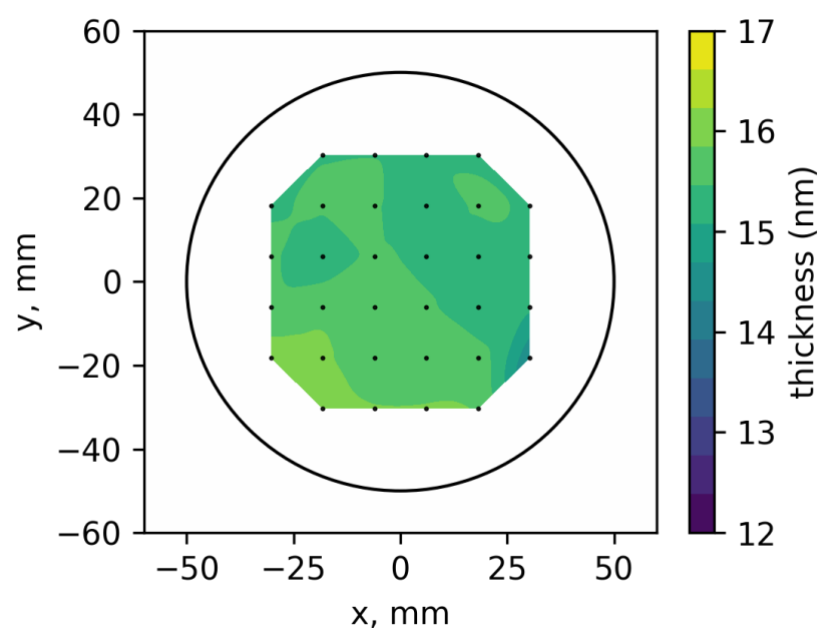


Figure S3i: Ellipsometrically determined areal thickness map of the 15.5 ± 0.3 nm PMETAC brush used for all *in situ* YCl_3 neutron reflectometry measurements.

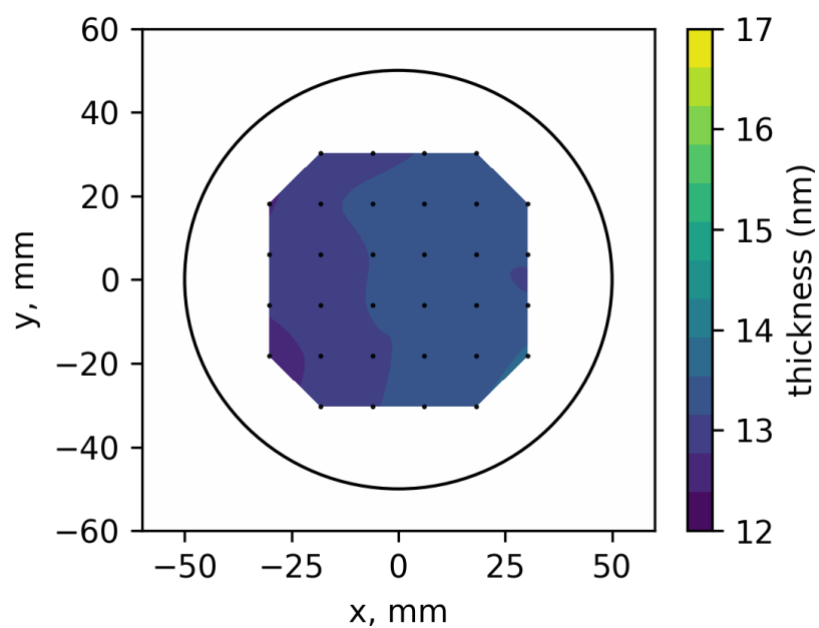


Figure S3ii: Ellipsometrically determined areal thickness map of the 13.1 ± 0.2 nm PMETAC brush used for all *in situ* KCl and LaCl_3 neutron reflectometry measurements.

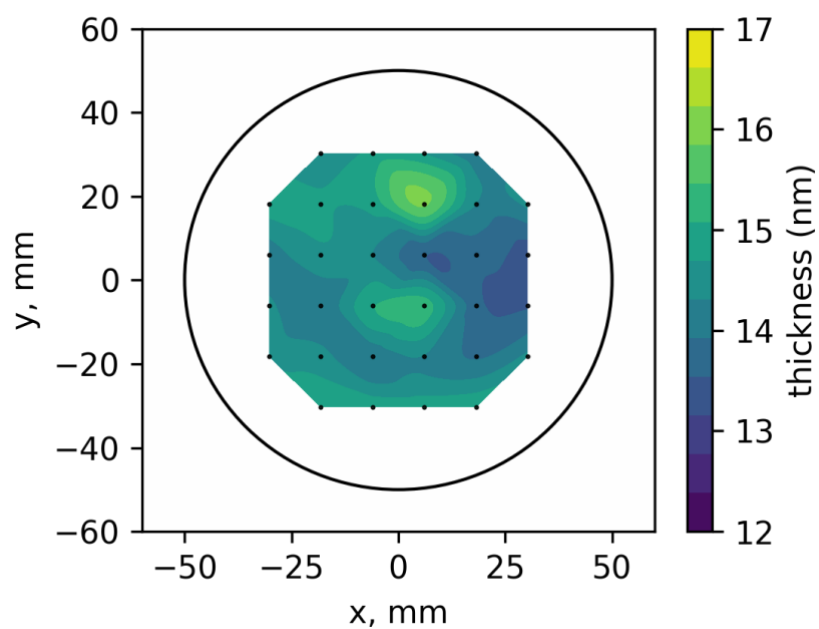


Figure S3iii: Ellipsometrically determined areal thickness map of the 14.4 ± 0.6 nm PMETAC brush used for all *in situ* MgCl_2 neutron reflectometry measurements.

In situ solid-liquid measurements

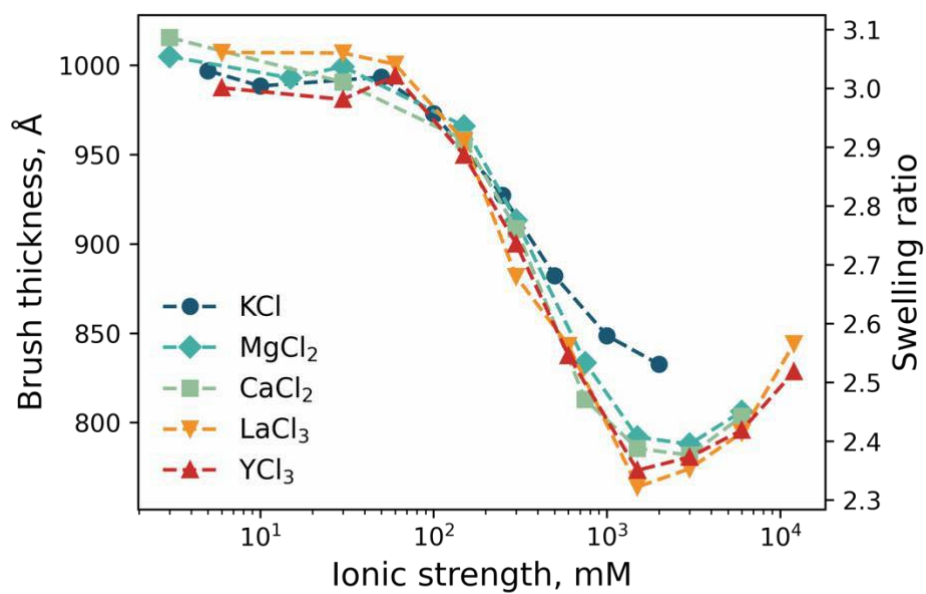


Figure S4: Solvated brush thickness (and resultant swelling ratio) of a PMETAC brush in various electrolytes of 1 mM to 2000 mM as a function of ionic strength. Reproduced using data from Figure 7.

Underscreening analysis

*

Here we provide a detailed explanation for the calculation of the effective screening length, λ_s , from spectroscopic ellipsometry data. The PMETAC brush in LaCl_3 electrolytes will be used for the purposes of this demonstration.

Defining the Debye-Hückel and re-entrant regions

For all *in situ* spectroscopic ellipsometry measurements, data is sliced into two regimes: the Debye-Hückel region and underscreening/re-entrant region. The Debye-Hückel region is defined as the region to which the brush thickness is monotonically decreasing with increasing electrolyte concentration. This region commences from the lowest salt concentration and continues to when the brush thickness reaches a minimum (Figure S5, yellow region). The re-entrant/underscreening region is the domain corresponding to all salt concentrations post minimum brush thickness (Figure S5, green region). The interface between yellow and green shaded areas in Figure S5 presents the “minimum” brush thickness. These two regions are best defined in Figure S5 which presents the brush thickness as a function of LaCl_3 concentration. Here the authors note that not all electrolytes imparted a “re-entrant regime” on the PMETAC brush.

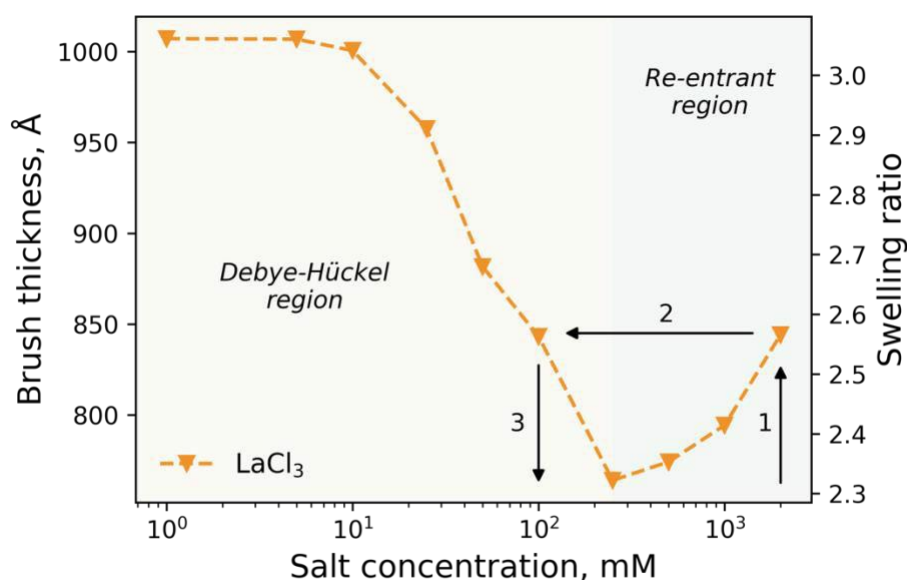


Figure S5: PMETAC brush thickness determined by spectroscopic ellipsometry in various LaCl_3 electrolytes. Reproduced from Figure 7. The yellow and green regions denote the Debye-Hückel and re-entrant regions, respectively. Arrows demonstrate brush thickness mapping from the re-entrant to Debye-Hückel region for λ_s^* analysis as discussed below.

Effective screening length calculation

Classically the screening length of a system is defined by:

$$\lambda_D = \sqrt{\frac{\epsilon_0 \epsilon_p k T}{e^2 \sum_i n_i z_i^2}} \quad (\text{S1})$$

where λ_D is the Debye-Hückel screening length, ϵ_0 is the permittivity of free space, ϵ_p is the relative permittivity, k is the Boltzmann constant, T is the absolute temperature, e is the elementary charge, n_i is the number density of ion i , and z_i is valency of ion i . For measurements across both regions, the

effective screening length is the experimentally determined screening length informed by ellipsometry measurements. For all measurements in the Debye-Hückel region, the behaviour of the brush can be explained by Debye-Hückel theory, whereby increasing the concentration of the electrolyte increases the charge screening in the polymer brush, leading to a decrease in electrolyte static repulsion and brush collapse. Importantly, for all electrolyte concentrations in the Debye-Hückel region, the Debye length is equal to the effective screening length, i.e., $\lambda_D = \lambda_s^*$. However, for the re-entrant region, this is not the case.

In order to determine λ_s^* for data within the re-entrant region, data was mapped into the Debye-Hückel region. Initially, an interpolating function was created using `scipy.interpolate.interp1d` based on the data in the Debye-Hückel region. The brush thickness data point in the re-entrant region was then mapped back (interpolated) into the Debye-Hückel region, by taking the brush thickness in the re-entrant region and deducing the salt concentration in the Debye-Hückel region which matches that brush thickness. This process is illustrated by arrows in Figure S5, which demonstrates how the brush thickness in 2 M LaCl_3 is mapped between regions in order to determine an “effective salt concentration”. This effective concentration was then used in Equation S1 to determine λ_s^* .

Scaling analysis

Using the determined effective scaling length (λ_s^*), a log-log plot of λ_s^*/λ_D vs a/λ_D was produced (Figure 9), where a is the mean diameter of the ion and λ_D is the screening length as determined from Debye-Hückel theory (Equation S1). Specifically, a was calculated by taking the sum of the mean anion and cation radii;⁸ reproducing the analysis by Lee et al.⁹ λ_D was determined using the *actual concentration*, not the *effective concentration*. From this log-log plot, the gradient of the linear region in the re-entrant regime (i.e., at very low λ_D) yields the scaling of underscreening present; the parameter ρ from Equation 4.

Neutron Reflectometry

First moment

For all neutron reflectometry data presented, the brush thickness can be extracted *via* the first moment (Equation 2) of the polymer VF profiles as presented in Figures 6 and S7. These results are presented in Figure S6.

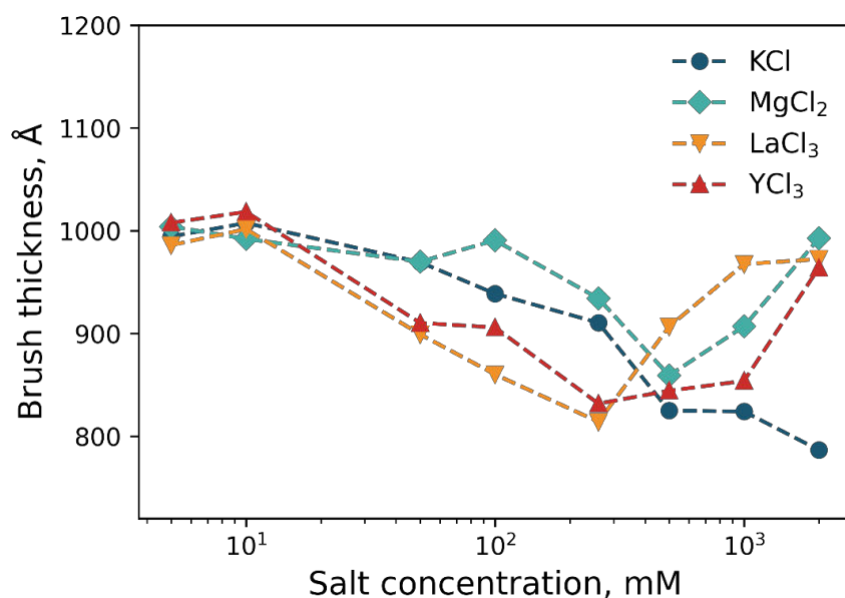


Figure S6: Neutron reflectometry derived polymer brush thickness of a PMETAC brush in various electrolytes. Brush thickness is deduced from twice the first moment of the VF profiles presented in Figures S7-11.

Full suite of NR data

Here we present the full suite of (a) neutron reflectometry data and the respective (b) SLD profiles and (c) polymer VF profiles for each electrolyte and concentration examined: (i) KCl; (ii) MgCl₂; (iii) LaCl₃; (iv) YCl₃.

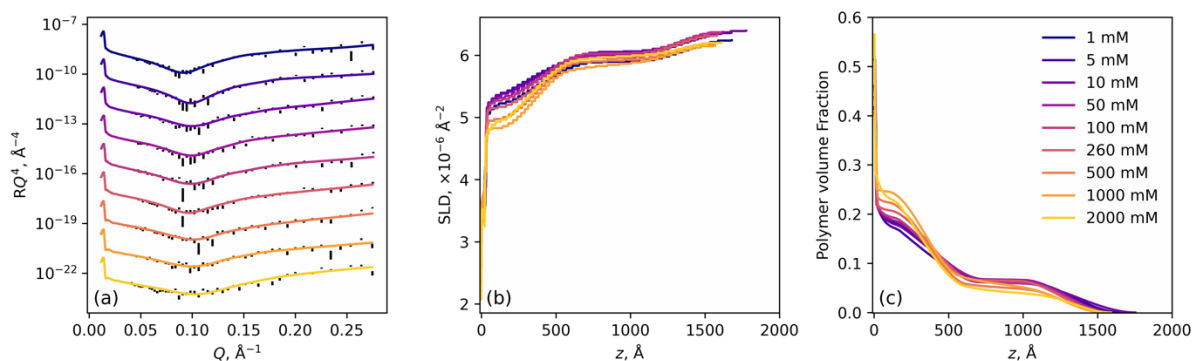


Figure S7i: (a) Neutron reflectivity and optimised model, (b) SLD profile and (c) polymer VF profiles for a PMETAC brush in KCl electrolytes of varying concentrations from 1 mM to 2000 mM.

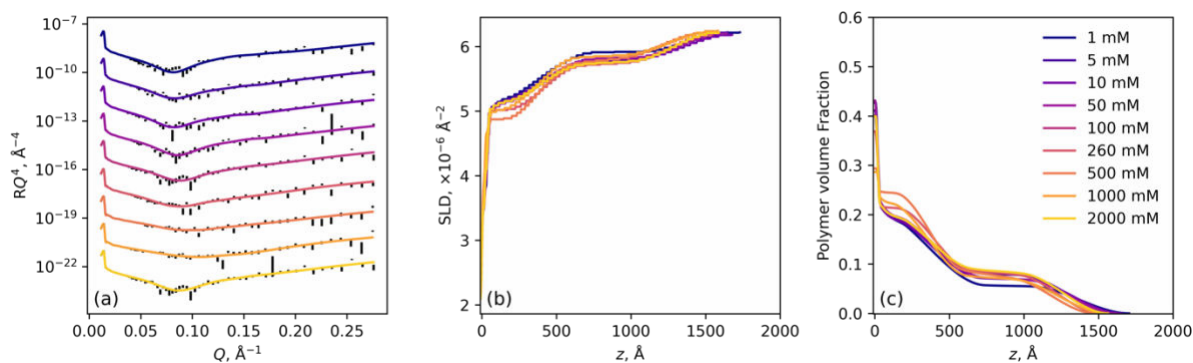


Figure S7ii: (a) Neutron reflectivity and optimised model, (b) SLD profile and (c) polymer VF profiles for a PMETAC brush in MgCl_2 electrolytes of varying concentrations from 1 mM to 2000 mM.

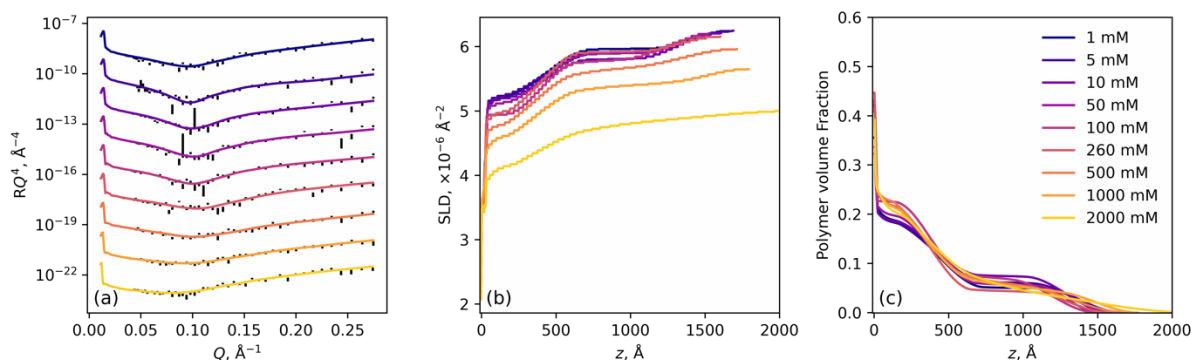


Figure S7iii: (a) Neutron reflectivity and optimised model, (b) SLD profile and (c) polymer VF profiles for a PMETAC brush in LaCl_3 electrolytes of varying concentrations from 1 mM to 2000 mM. In (b), the reduced solvent SLD, compared to pure D_2O , are the result of the salt-bound hydrogenated water molecules.

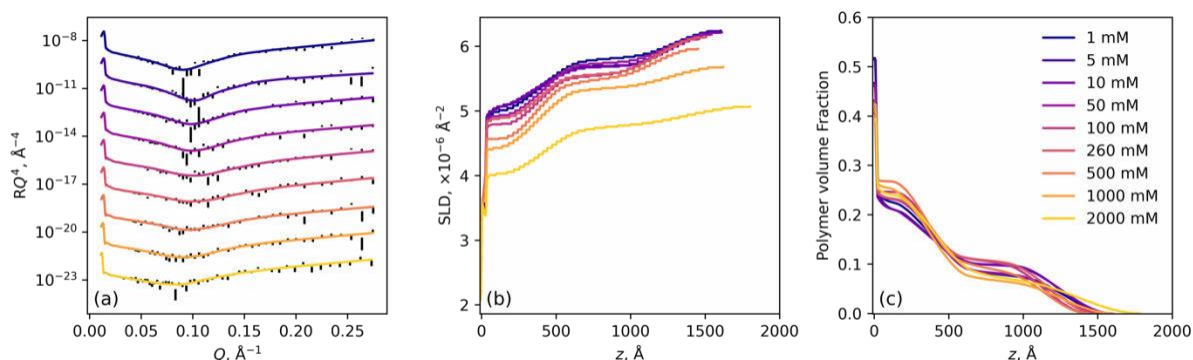


Figure S7iv: (a) Neutron reflectivity and optimised model, (b) SLD profile and (c) polymer VF profiles for a PMETAC brush in YCl_3 electrolytes of varying concentrations from 1 mM to 2000 mM. In (b), the reduced solvent SLD, compared to pure D_2O , are the result of the salt-bound hydrogenated water molecules.

MCMC spread of fits

Here we present the MCMC derived distribution of fits for a PMETAC brush in various concentrations of KCl (Figure S8); MgCl₂ (Figure S9), LaCl₃ (Figure S10) and YCl₃ (Figure S11).

KCl

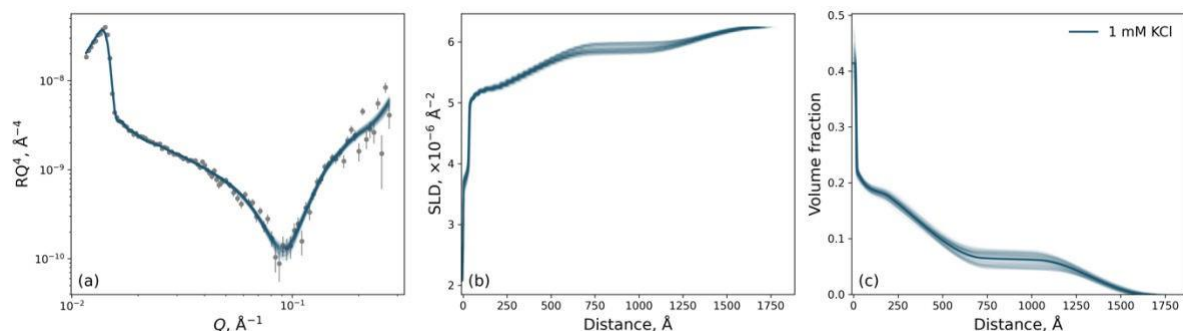


Figure S8i: (a) Optimised model for a PMETAC brush in 1 mM KCl: (a) experimental and modelled reflectivity, (b) scattering length density profile, and (c) polymer volume fraction profile. Distribution of fits is derived from the MCMC sampling of the posterior distribution function.

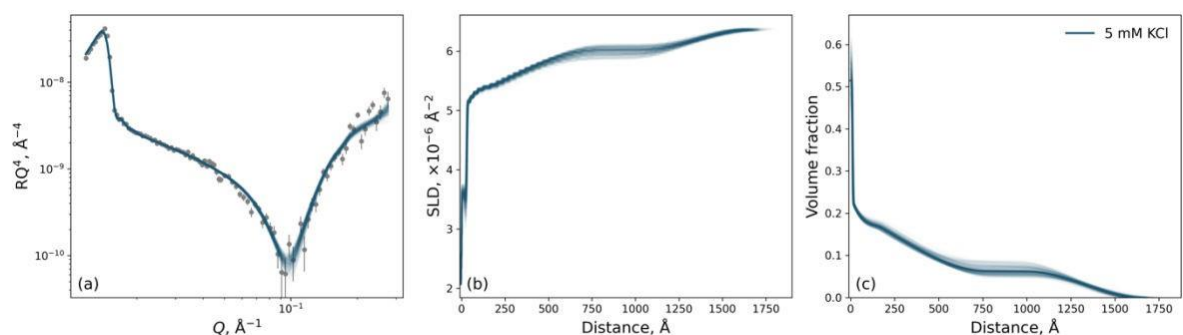


Figure S8ii: (a) Optimised model for a PMETAC brush in 5 mM KCl: (a) experimental and modelled reflectivity, (b) scattering length density profile, and (c) polymer volume fraction profile. Distribution of fits is derived from the MCMC sampling of the posterior distribution function.

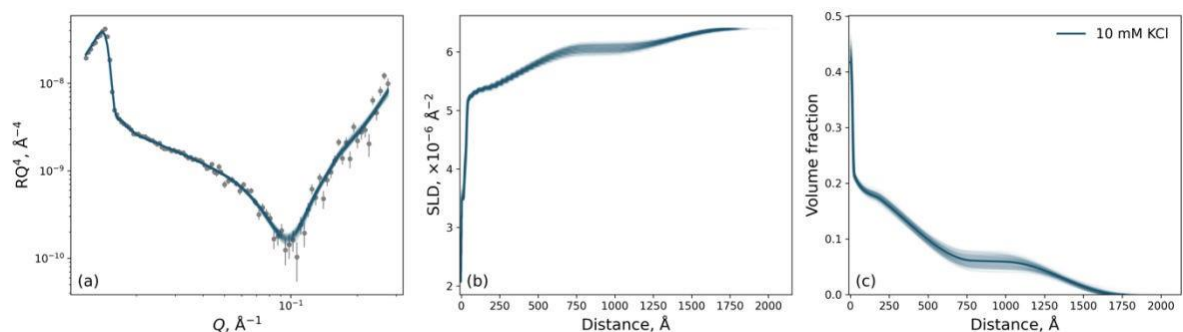


Figure S8iii: (a) Optimised model for a PMETAC brush in 10 mM KCl: (a) experimental and modelled reflectivity, (b) scattering length density profile, and (c) polymer volume fraction profile. Distribution of fits is derived from the MCMC sampling of the posterior distribution function.

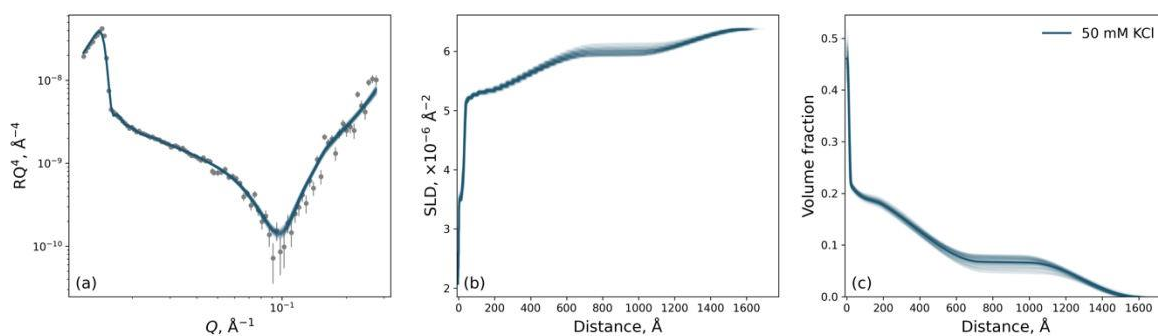


Figure S8iv: (a) Optimised model for a PMETAC brush in 50 mM KCl: (a) experimental and modelled reflectivity, (b) scattering length density profile, and (c) polymer volume fraction profile. Distribution of fits is derived from the MCMC sampling of the posterior distribution function.

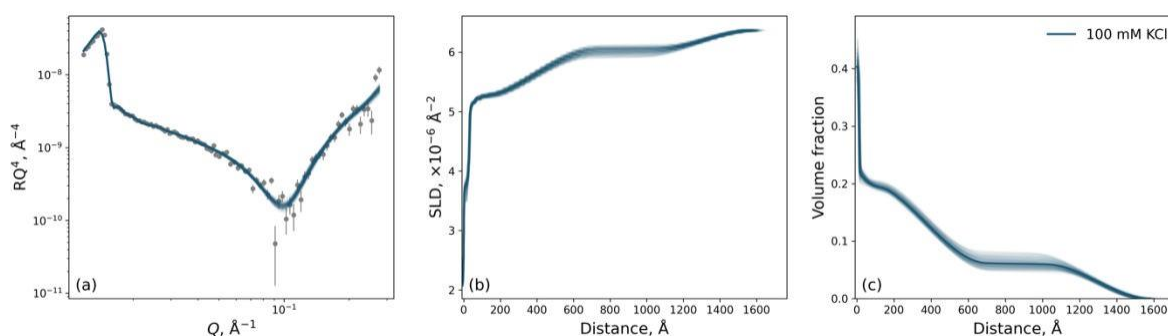


Figure S8v: (a) Optimised model for a PMETAC brush in 100 mM KCl: (a) experimental and modelled reflectivity, (b) scattering length density profile, and (c) polymer volume fraction profile. Distribution of fits is derived from the MCMC sampling of the posterior distribution function.

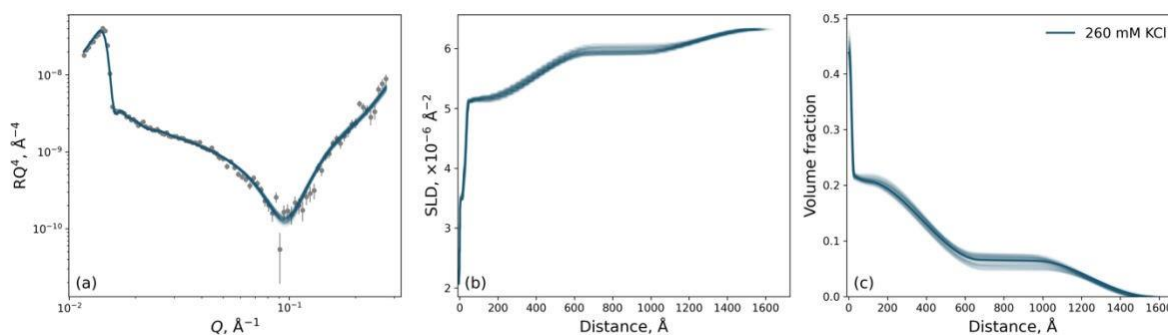


Figure S8vi: (a) Optimised model for a PMETAC brush in 260 mM KCl: (a) experimental and modelled reflectivity, (b) scattering length density profile, and (c) polymer volume fraction profile. Distribution of fits is derived from the MCMC sampling of the posterior distribution function.

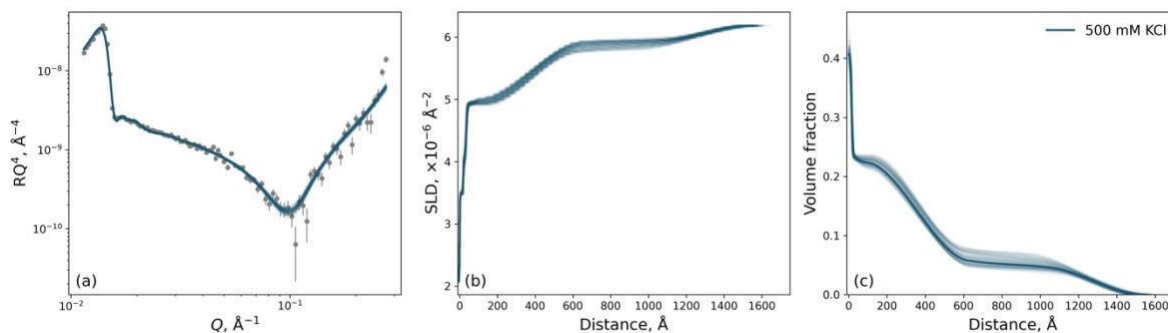


Figure S8vii: (a) Optimised model for a PMETAC brush in 500 mM KCl: (a) experimental and modelled reflectivity, (b) scattering length density profile, and (c) polymer volume fraction profile. Distribution of fits is derived from the MCMC sampling of the posterior distribution function.

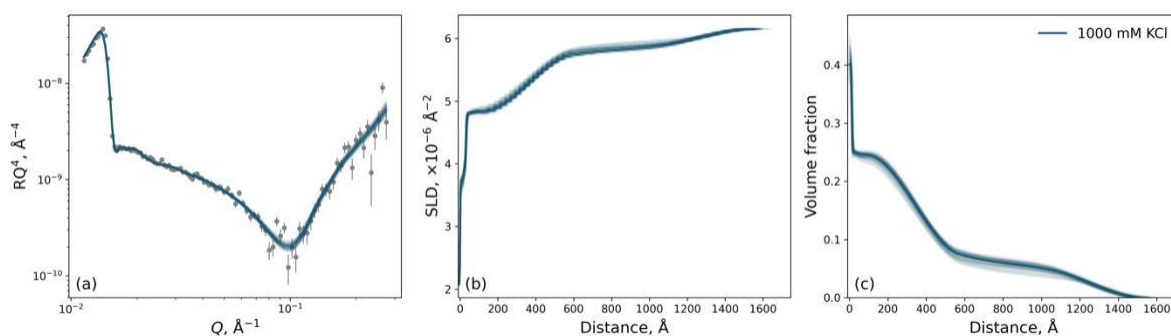


Figure S8viii: (a) Optimised model for a PMETAC brush in 1000 mM KCl: (a) experimental and modelled reflectivity, (b) scattering length density profile, and (c) polymer volume fraction profile. Distribution of fits is derived from the MCMC sampling of the posterior distribution function.

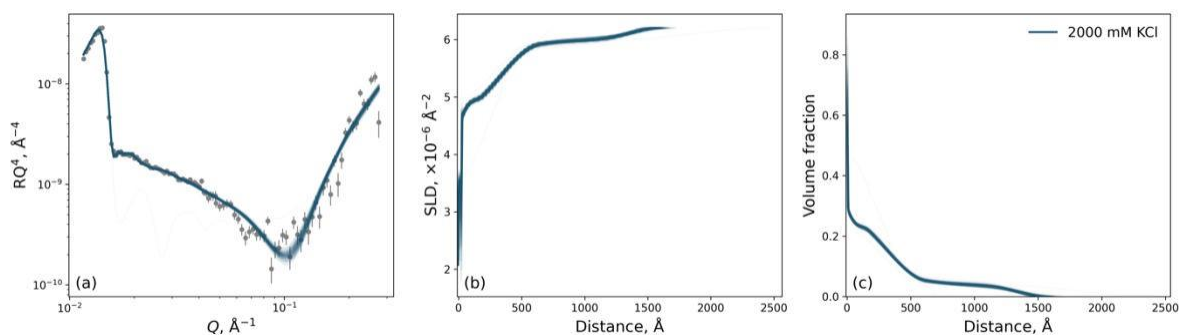


Figure S8ix: (a) Optimised model for a PMETAC brush in 2000 mM KCl: (a) experimental and modelled reflectivity, (b) scattering length density profile, and (c) polymer volume fraction profile. Distribution of fits is derived from the MCMC sampling of the posterior distribution function.

MgCl₂

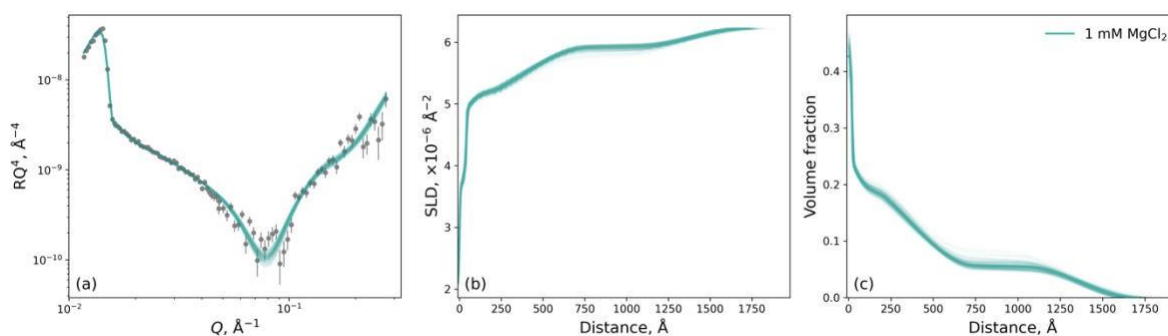


Figure S9i: (a) Optimised model for a PMETAC brush in 1 mM MgCl₂: (a) experimental and modelled reflectivity, (b) scattering length density profile, and (c) polymer volume fraction profile. Distribution of fits is derived from the MCMC sampling of the posterior distribution function.

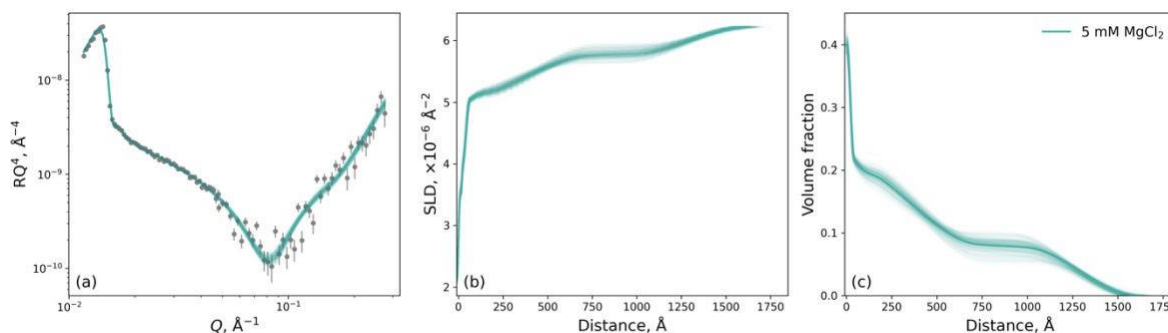


Figure S9ii: (a) Optimised model for a PMETAC brush in 5 mM MgCl₂: (a) experimental and modelled reflectivity, (b) scattering length density profile, and (c) polymer volume fraction profile. Distribution of fits is derived from the MCMC sampling of the posterior distribution function.

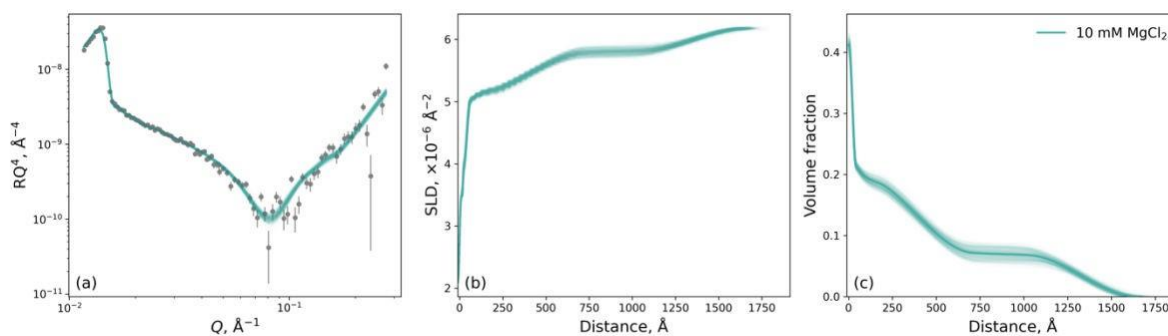


Figure S9iii: (a) Optimised model for a PMETAC brush in 10 mM MgCl₂: (a) experimental and modelled reflectivity, (b) scattering length density profile, and (c) polymer volume fraction profile. Distribution of fits is derived from the MCMC sampling of the posterior distribution function.

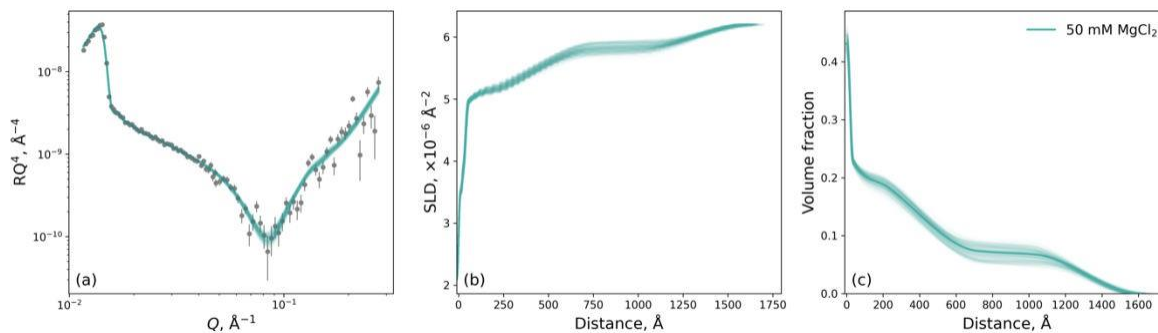


Figure S9iv: (a) Optimised model for a PMETAC brush in 50 mM MgCl_2 : (a) experimental and modelled reflectivity, (b) scattering length density profile, and (c) polymer volume fraction profile. Distribution of fits is derived from the MCMC sampling of the posterior distribution function.

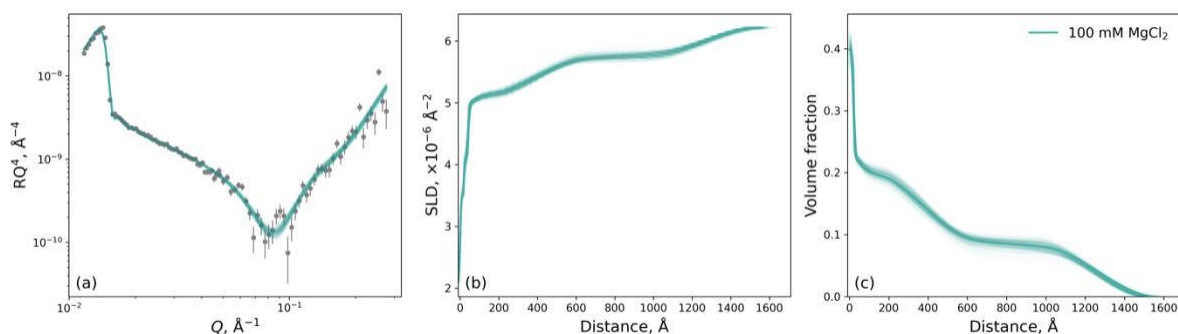


Figure S9v: (a) Optimised model for a PMETAC brush in 100 mM MgCl_2 : (a) experimental and modelled reflectivity, (b) scattering length density profile, and (c) polymer volume fraction profile. Distribution of fits is derived from the MCMC sampling of the posterior distribution function.

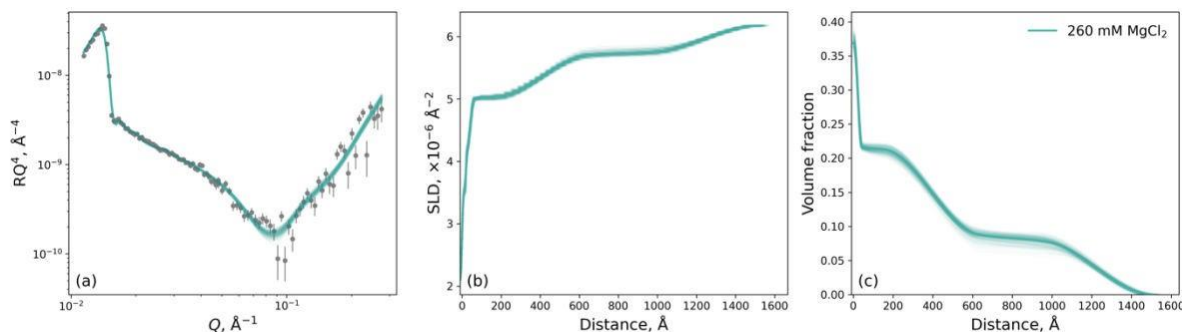


Figure S9vi: (a) Optimised model for a PMETAC brush in 260 mM MgCl_2 : (a) experimental and modelled reflectivity, (b) scattering length density profile, and (c) polymer volume fraction profile. Distribution of fits is derived from the MCMC sampling of the posterior distribution function.

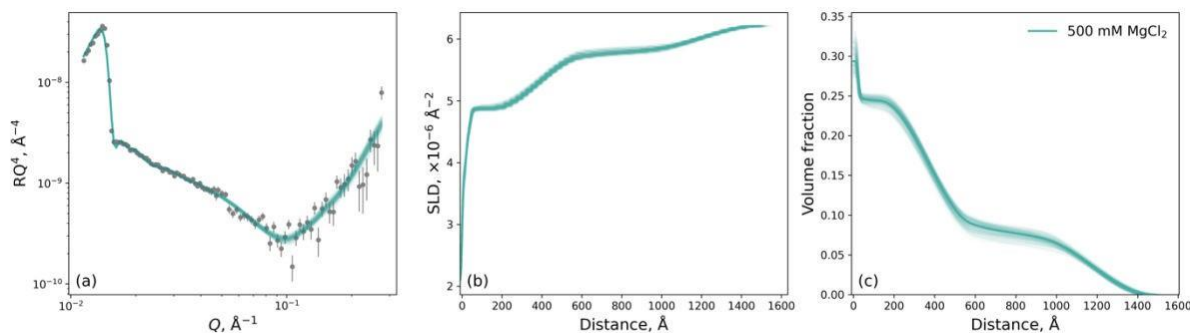


Figure S9vii: (a) Optimised model for a PMETAC brush in 500 mM MgCl_2 : (a) experimental and modelled reflectivity, (b) scattering length density profile, and (c) polymer volume fraction profile. Distribution of fits is derived from the MCMC sampling of the posterior distribution function.

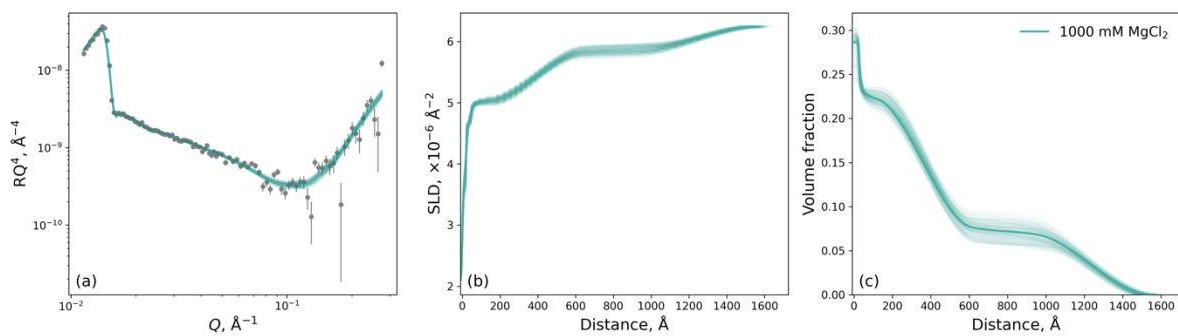


Figure S9viii: (a) Optimised model for a PMETAC brush in 1000 mM MgCl_2 : (a) experimental and modelled reflectivity, (b) scattering length density profile, and (c) polymer volume fraction profile. Distribution of fits is derived from the MCMC sampling of the posterior distribution function.

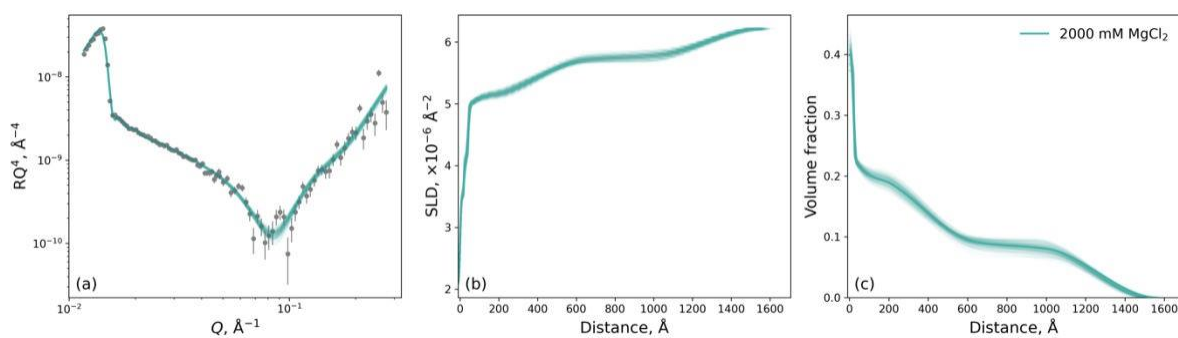


Figure S9ix: (a) Optimised model for a PMETAC brush in 2000 mM MgCl_2 : (a) experimental and modelled reflectivity, (b) scattering length density profile, and (c) polymer volume fraction profile. Distribution of fits is derived from the MCMC sampling of the posterior distribution function.

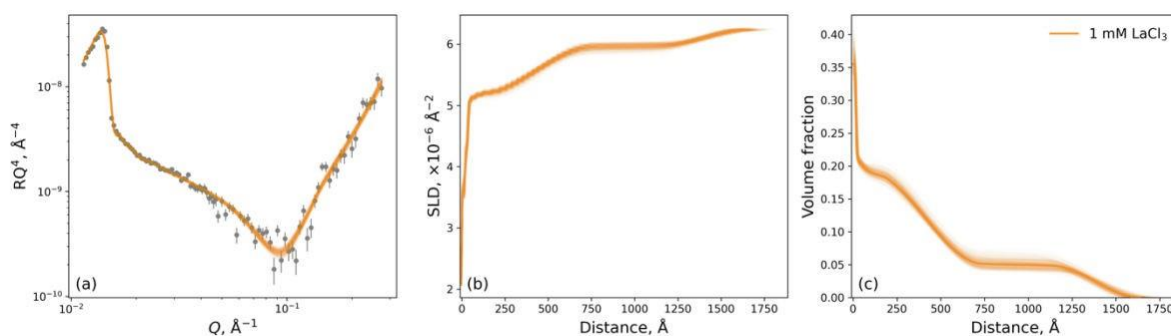


Figure S10i: (a) Optimised model for a PMETAC brush in 1 mM LaCl₃: (a) experimental and modelled reflectivity, (b) scattering length density profile, and (c) polymer volume fraction profile. Distribution of fits is derived from the MCMC sampling of the posterior distribution function.

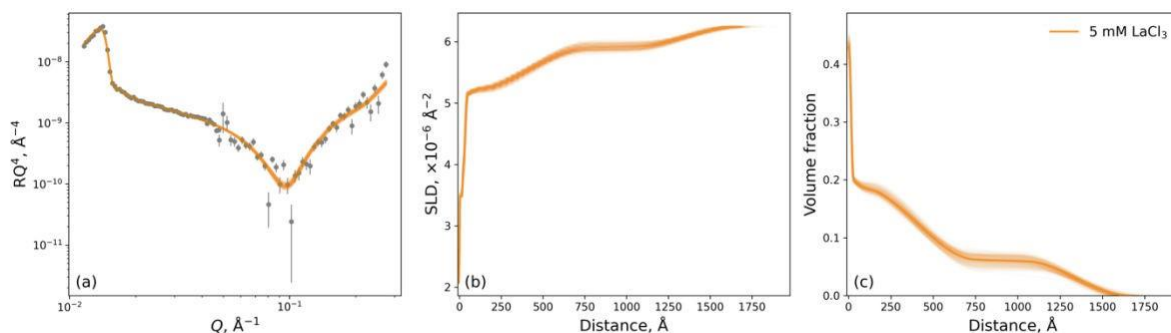


Figure S10ii: (a) Optimised model for a PMETAC brush in 5 mM LaCl₃: (a) experimental and modelled reflectivity, (b) scattering length density profile, and (c) polymer volume fraction profile. Distribution of fits is derived from the MCMC sampling of the posterior distribution function.

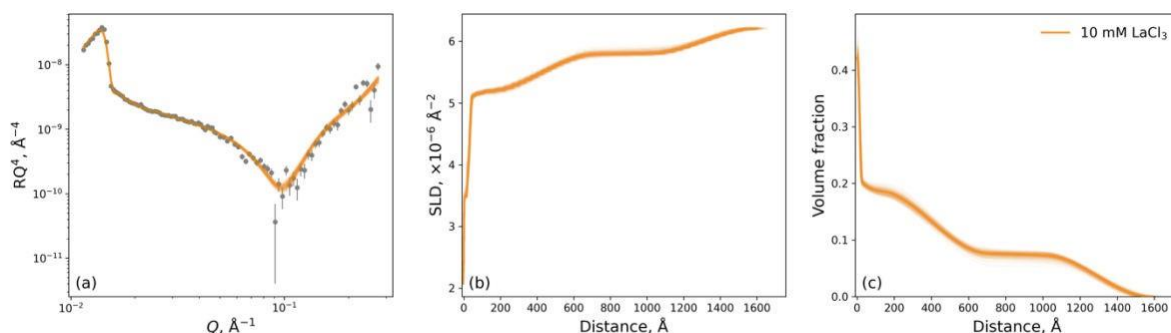


Figure S10iii: (a) Optimised model for a PMETAC brush in 10 mM LaCl₃: (a) experimental and modelled reflectivity, (b) scattering length density profile, and (c) polymer volume fraction profile. Distribution of fits is derived from the MCMC sampling of the posterior distribution function.

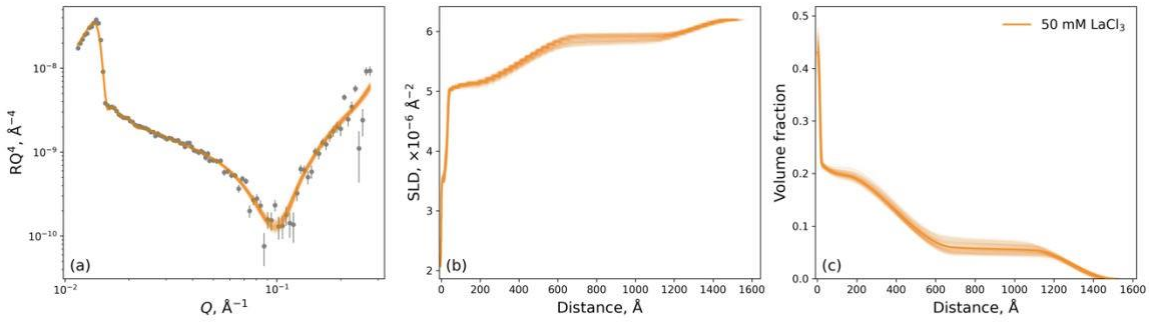


Figure S10iv: (a) Optimised model for a PMETAC brush in 50 mM LaCl_3 : (a) experimental and modelled reflectivity, (b) scattering length density profile, and (c) polymer volume fraction profile. Distribution of fits is derived from the MCMC sampling of the posterior distribution function.

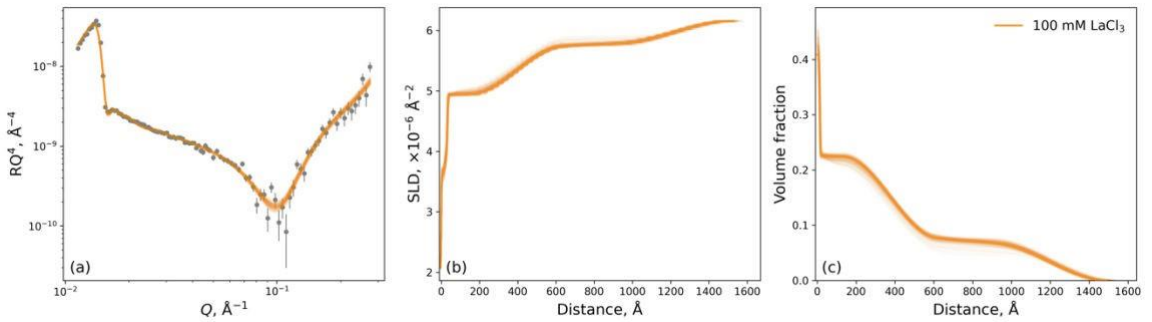


Figure S10v: (a) Optimised model for a PMETAC brush in 100 mM LaCl_3 : (a) experimental and modelled reflectivity, (b) scattering length density profile, and (c) polymer volume fraction profile. Distribution of fits is derived from the MCMC sampling of the posterior distribution function.

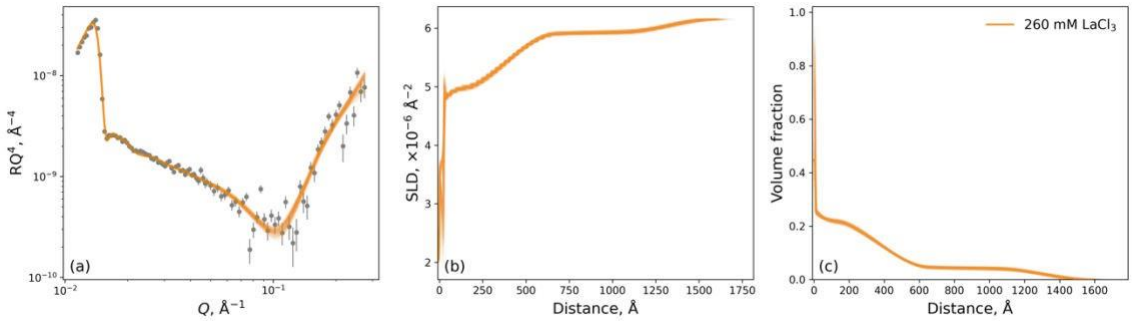


Figure S10vi: (a) Optimised model for a PMETAC brush in 260 mM LaCl_3 : (a) experimental and modelled reflectivity, (b) scattering length density profile, and (c) polymer volume fraction profile. Distribution of fits is derived from the MCMC sampling of the posterior distribution function.

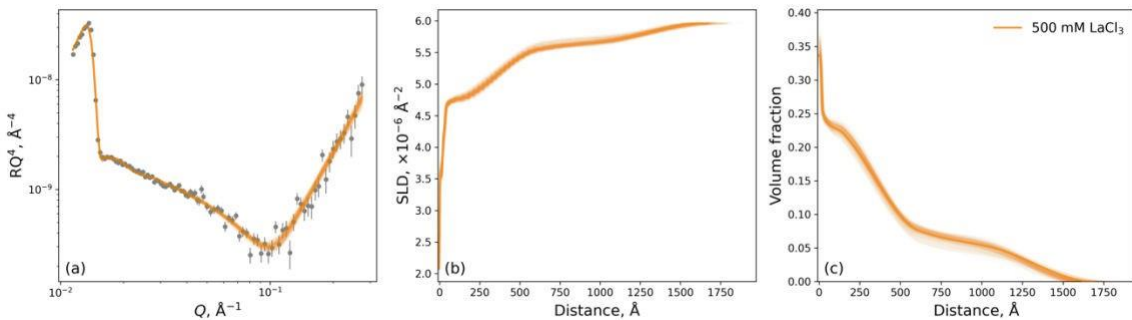


Figure S10vii: (a) Optimised model for a PMETAC brush in 500 mM LaCl_3 : (a) experimental and modelled reflectivity, (b) scattering length density profile, and (c) polymer volume fraction profile. Distribution of fits is derived from the MCMC sampling of the posterior distribution function.

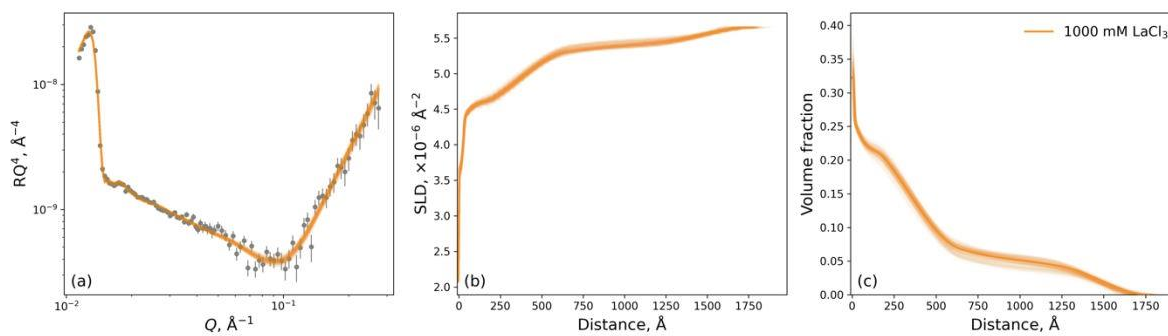


Figure S10viii: (a) Optimised model for a PMETAC brush in 1000 mM LaCl_3 : (a) experimental and modelled reflectivity, (b) scattering length density profile, and (c) polymer volume fraction profile. Distribution of fits is derived from the MCMC sampling of the posterior distribution function.

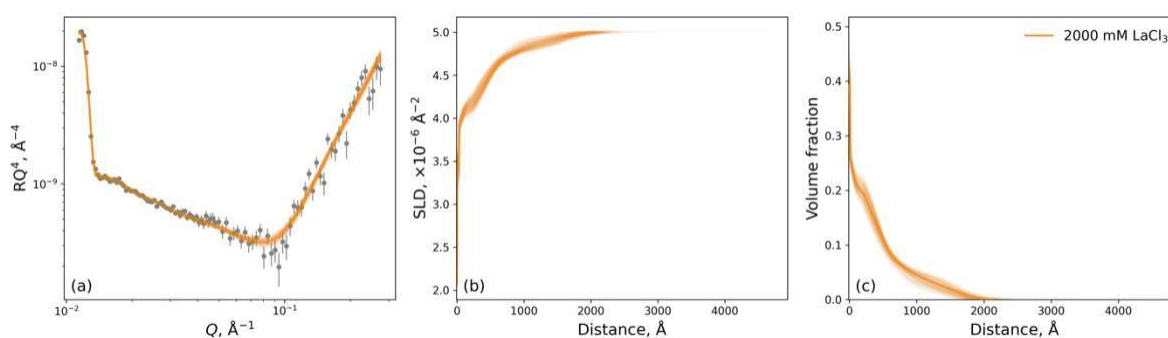


Figure S10ix: (a) Optimised model for a PMETAC brush in 2000 mM LaCl_3 : (a) experimental and modelled reflectivity, (b) scattering length density profile, and (c) polymer volume fraction profile. Distribution of fits is derived from the MCMC sampling of the posterior distribution function.

YCl₃

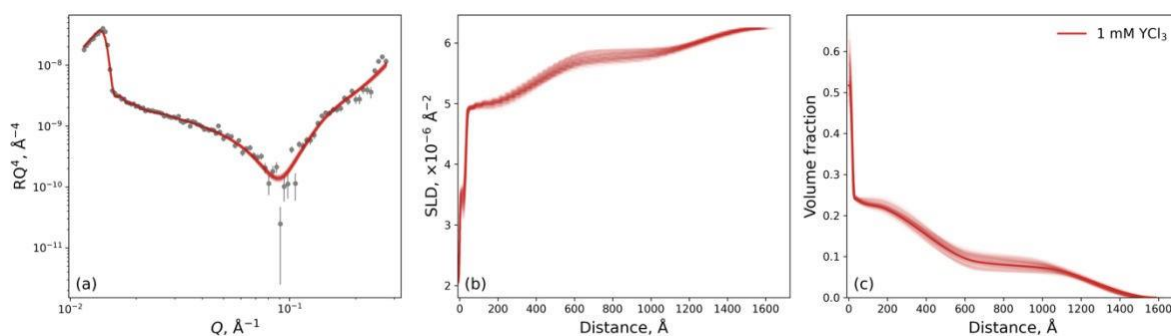


Figure S11i: (a) Optimised model for a PMETAC brush in 1 mM YCl₃: (a) experimental and modelled reflectivity, (b) scattering length density profile, and (c) polymer volume fraction profile. Distribution of fits is derived from the MCMC sampling of the posterior distribution function.

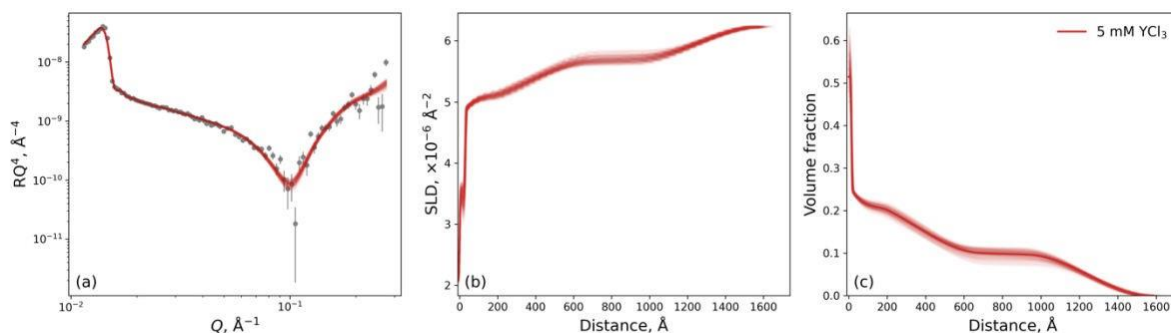


Figure S11ii: (a) Optimised model for a PMETAC brush in 5 mM YCl₃: (a) experimental and modelled reflectivity, (b) scattering length density profile, and (c) polymer volume fraction profile. Distribution of fits is derived from the MCMC sampling of the posterior distribution function.

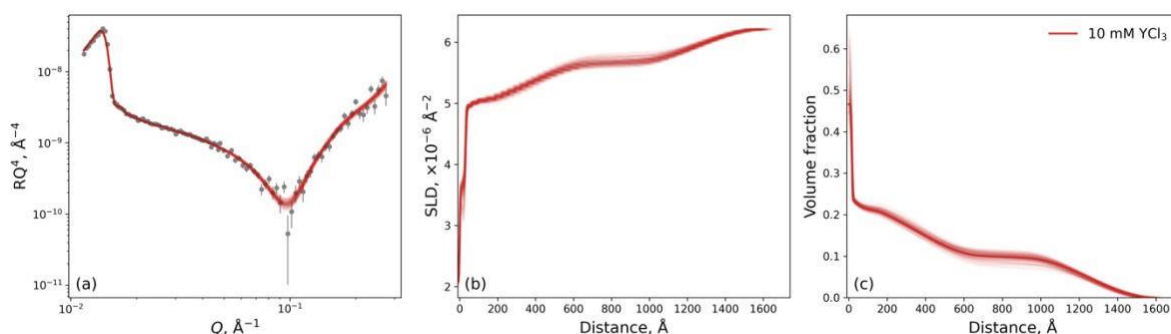


Figure S11iii: (a) Optimised model for a PMETAC brush in 10 mM YCl₃: (a) experimental and modelled reflectivity, (b) scattering length density profile, and (c) polymer volume fraction profile. Distribution of fits is derived from the MCMC sampling of the posterior distribution function.

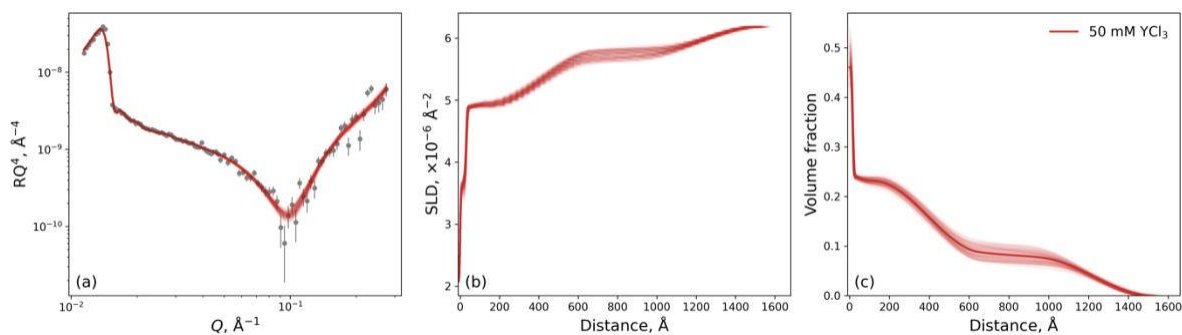


Figure S11iv: (a) Optimised model for a PMETAC brush in 50 mM YCl_3 : (a) experimental and modelled reflectivity, (b) scattering length density profile, and (c) polymer volume fraction profile. Distribution of fits is derived from the MCMC sampling of the posterior distribution function.

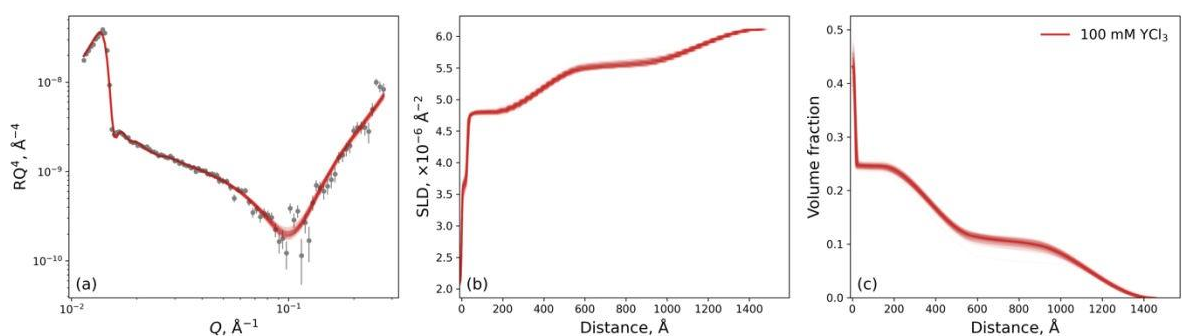


Figure S11v: (a) Optimised model for a PMETAC brush in 100 mM YCl_3 : (a) experimental and modelled reflectivity, (b) scattering length density profile, and (c) polymer volume fraction profile. Distribution of fits is derived from the MCMC sampling of the posterior distribution function.

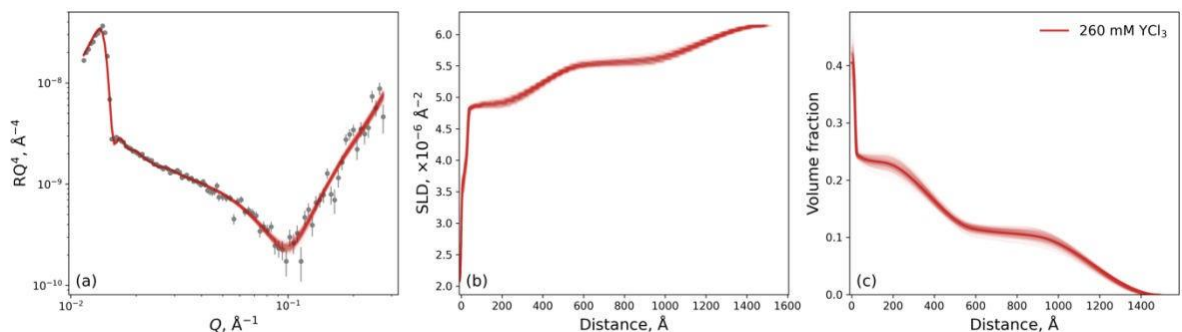


Figure S11vi: (a) Optimised model for a PMETAC brush in 260 mM YCl_3 : (a) experimental and modelled reflectivity, (b) scattering length density profile, and (c) polymer volume fraction profile. Distribution of fits is derived from the MCMC sampling of the posterior distribution function.

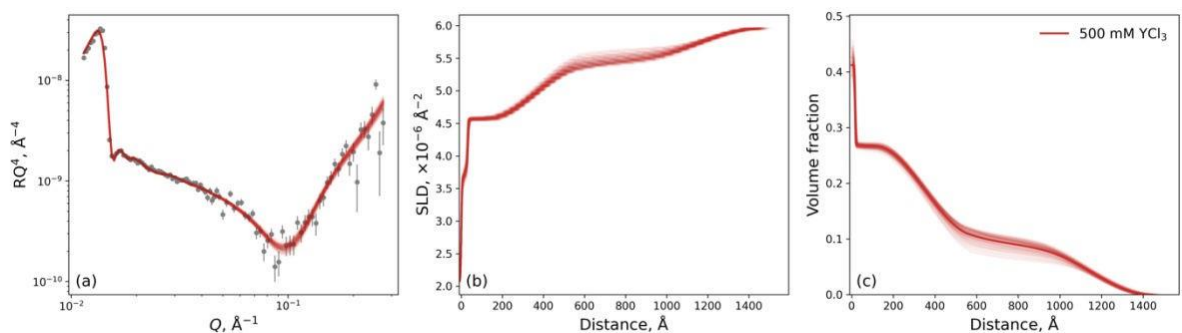


Figure S11vii: (a) Optimised model for a PMETAC brush in 500 mM YCl_3 : (a) experimental and modelled reflectivity, (b) scattering length density profile, and (c) polymer volume fraction profile. Distribution of fits is derived from the MCMC sampling of the posterior distribution function.

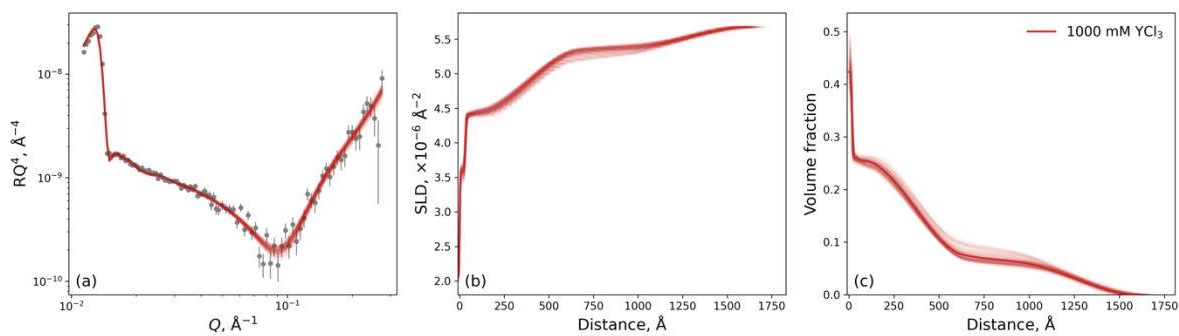


Figure S11viii: (a) Optimised model for a PMETAC brush in 1000 mM YCl_3 : (a) experimental and modelled reflectivity, (b) scattering length density profile, and (c) polymer volume fraction profile. Distribution of fits is derived from the MCMC sampling of the posterior distribution function.

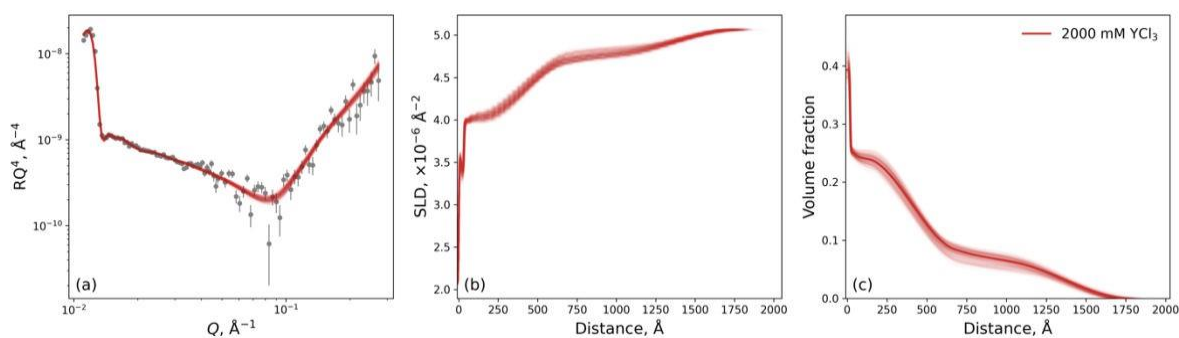


Figure S11ix: (a) Optimised model for a PMETAC brush in 2000 mM YCl_3 : (a) experimental and modelled reflectivity, (b) scattering length density profile, and (c) polymer volume fraction profile. Distribution of fits is derived from the MCMC sampling of the posterior distribution function.

References

- 1 J. Ralston, I. Larson, M. W. Rutland, A. A. Feiler and M. Kleijn, Atomic force microscopy and direct surface force measurements (IUPAC technical report), *Pure Appl. Chem.*, 2005, **77**, 2149–2170.
- 2 H. J. Butt, B. Cappella and M. Kappl, Force measurements with the atomic force microscope: Technique, interpretation and applications, *Surf. Sci. Rep.*, 2005, **59**, 1–152.
- 3 J. D. Willott, T. J. Murdoch, G. B. Webber and E. J. Wanless, Nature of the Specific Anion Response of a Hydrophobic Weak Polyelectrolyte Brush Revealed by AFM Force Measurements, *Macromolecules*, 2016, **49**, 2327–2338.
- 4 H. Robertson, J. D. Willott, K. P. Gregory, E. C. Johnson, I. J. Gresham, A. R. J. Nelson, V. S. J. Craig, S. W. Prescott, R. Chapman, G. B. Webber and E. J. Wanless, From Hofmeister to hydrotrope: Effect of anion hydrocarbon chain length on a polymer brush, *J. Colloid Interface Sci.*, 2023, **634**, 983–994.
- 5 H. Robertson, I. J. Gresham, S. W. Prescott, G. B. Webber, E. J. Wanless and A. Nelson, refellips: A Python package for the analysis of variable angle spectroscopic ellipsometry data, *SoftwareX*, 2022, **20**, 101225.
- 6 H. Robertson, I. J. Gresham, S. W. Prescott, G. B. Webber, E. J. Wanless and A. Nelson, refellips: A Python package for the analysis of variable angle spectroscopic ellipsometry data, *SoftwareX*, , DOI:10.1016/j.softx.2022.101225.
- 7 H. Robertson, A. R. J. Nelson, G. B. Webber, S. W. Prescott, V. S. J. Craig, E. J. Wanless and J. D. Willott, Supporting information for ‘Underscreening in concentrated electrolytes: Polyelectrolyte brushes exhibit re-entrant swelling behaviour’, *Zenodo*, 2023, DOI: 10.5281/zenodo.7743201.
- 8 R. Shannon, Revised effective ionic radii and systematic studies of interatomic distances in halides and chalcogenides, *Acta Crystallogr. Sect. A*, 1976, **32**, 751–767.
- 9 A. A. Lee, C. S. Perez-Martinez, A. M. Smith and S. Perkin, Scaling Analysis of the Screening Length in Concentrated Electrolytes, *Phys. Rev. Lett.*, 2017, **119**, 1–6.